Tetrahedron 65 (2009) 7277–7288

Contents lists available at ScienceDirect

Tetrahedron

journal homepage: www.elsevier.com/locate/tet

Chiral photochemistry in a confined space: torquoselective photoelectrocyclization of pyridones within an achiral hydrophobic capsule

Arun Kumar Sundaresan [a], Corinne L.D. Gibb [b], Bruce C. Gibb [b], V. Ramamurthy [a,*]

[a] Department of Chemistry, University of Miami, Coral Gables, FL 33124, USA
[b] Department of Chemistry, University of New Orleans, New Orleans, LA 70148, USA

ARTICLE INFO

Article history:
Received 13 November 2008
Accepted 21 January 2009
Available online 21 March 2009

On the occasion of 70th birthday V.R. dedicates this manuscript to his beloved mentor and teacher Professor R. S. H. Liu

Keywords:
Host–guest
Chiral photochemistry
Electrocyclization
Pyridones
Confined space
Supramolecular assemblies

ABSTRACT

Chiral induction during the photoelectrocyclization of pyridones included within octa acid (OA) capsule has been established. Chiral induction is brought about by a chiral auxiliary appended to the reactive pyridone moiety. Importantly, the same chiral auxiliary while ineffective in acetonitrile solution is found to be effective within the confined space of OA capsule. The diastereomeric excess of 92% obtained here is comparable only to that in solid state. OA capsule, we believe, provides restriction to the rotational motions of the reactant pyridone and chiral auxiliary and thus places the chiral auxiliary in a selective conformation with respect to the reactive pyridone part. A correlation between the position of the methyl group on the pyridone ring and diastereoselectivity was noted. Structures of the host–guest complexes were examined by ^{1}H NMR and the data were used to obtain preliminary information concerning the mechanism of chiral induction within the confined spaces of OA capsule.

1. Introduction

Chiral chemistry in confined spaces has attracted considerable attention during the last two decades.[1] Although a number of elegant and efficient chiral induction strategies have evolved for thermal reactions, the short lifetimes of excited states have hampered the development of effective interaction between excited reactant and a chiral perturber thus slowing down similar progress with photoreactions. The chiral sources that have been employed to achieve stereoselectivity in photochemical reactions in solution include circularly polarized light, chiral-sensitizers, -solvents, -substituents, and -hosts.[2–6] During the last two decades supramolecular approaches toward chiral photochemistry have attracted considerable attention. For example, use of chiral hosts such as cyclodextrins, proteins, and DNA to complex achiral reactant molecules in aqueous solution has resulted in low to moderate chiral induction in photoproducts, but significantly higher than in isotropic solvents.[4]

In comparison to solution, supramolecular approaches in the solid state have provided promising leads. Solid host–guest complexes of optically pure host and achiral guest molecules often resulted in quantitative chiral induction.[7] The elegant technique of transformation of chiral crystals of achiral molecules into chiral photoproducts in 100% enantiomeric excess (ee) is noteworthy.[8] Some achiral molecules that failed to crystallize in a chiral space group were forced to crystallize in a chiral space group by using an ionic or a co-valent chiral auxiliary and which upon subsequent irradiation yielded products with 100% diastereomeric excess (de).[9] We have recently demonstrated the use of confined cavities of a zeolite and the resident charge compensating cations in inducing enantio- and diastereoselectivities in products of photoreactions such as geometric isomerization, hydrogen abstraction, and cyclization.[10] Based on the literature, we believe that solid-state chiral photochemistry is more advanced than the solution counterpart and we should apply the solid-state concepts to solution chiral photochemistry. In this context the supramolecular approach in solution holds promise.

We had explored the use of chiral cyclodextrins as hosts for a number of unimolecular photoreactions toward developing a solution-based chiral induction strategy.[11–13] The best ~20% ee we could obtain in solution is largely due to cyclodextrin–guest complexes' poor solubility in water. The similarities in shape and size of cyclodextrins and the recently synthesized cavitand octa acid (OA) led us to explore OA's effectiveness in

* Corresponding author.
E-mail address: murthy1@miami.edu (V. Ramamurthy).

0040-4020/$ – see front matter © 2009 Elsevier Ltd. All rights reserved.
doi:10.1016/j.tet.2009.01.110

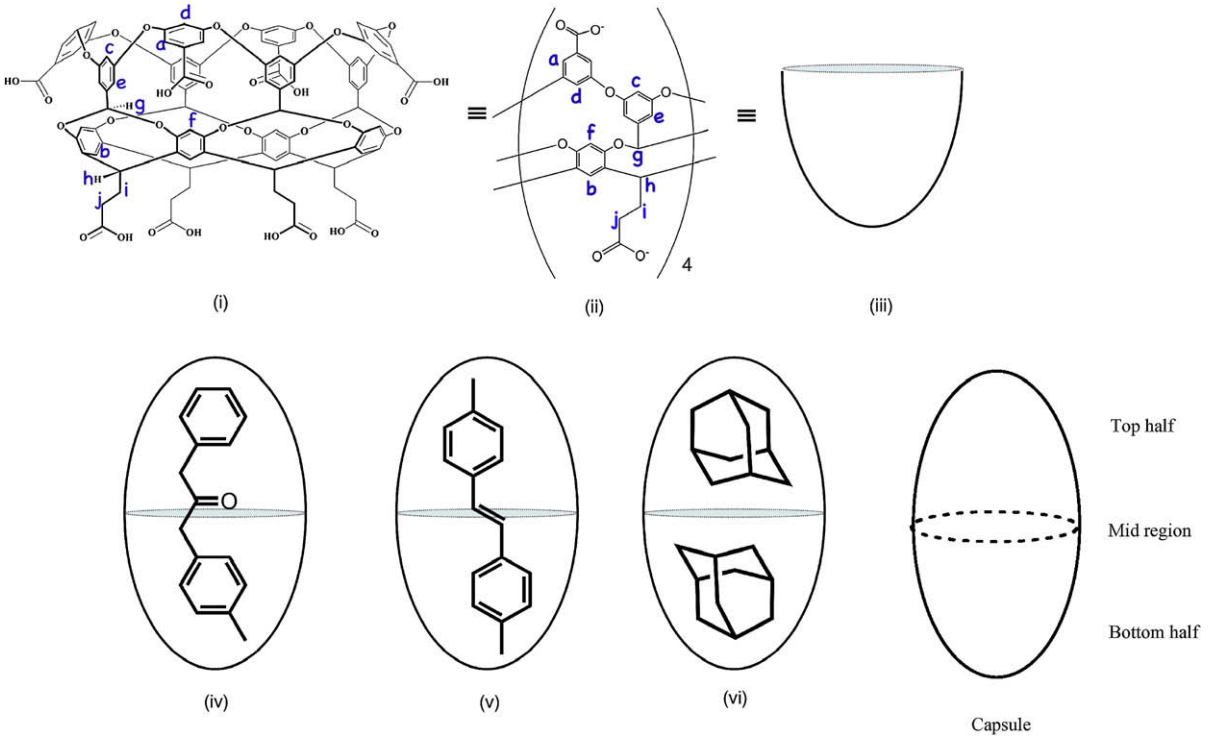

Figure 1. (i) Chemical structure of cavitand octa acid (OA). (ii) Simplified representation showing the 4 equiv subunits of OA. (iii) Cartoon representation of OA cavity. (iv)–(vi) Cartoon representation of 2:1 host–guest complexes formed with OA and 4-methyl dibenzyl ketone, 4,4′-dimethylstilbene and 2:2 host/guest complex with adamantane.

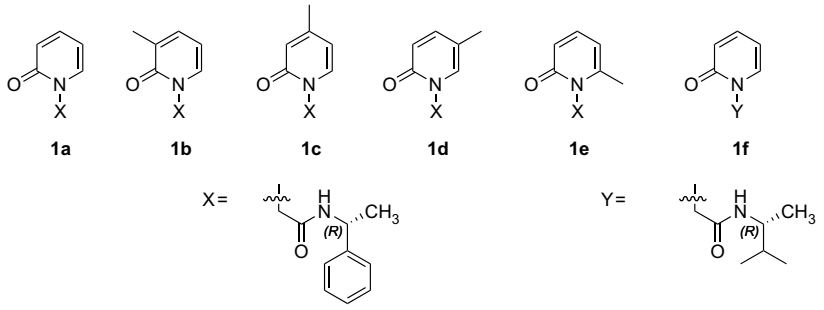

Scheme 1. Structures of pyridones examined in this study.

bringing about chiral induction in photoreactions. While the guest is only partially surrounded by cyclodextrin (as 1:1 guest@host complex), two molecules of OA self-assemble and encapsulate the guest (as either a 2:2 or a 1:2 guest@host capsule) (Fig. 1).[14,15] Thus the OA capsule provides a relatively 'confined-solid-like' reaction cavity resembling crystals and zeolites. Our experience with the latter two solid media suggested that the restriction provided by a closed tight enclosure would enhance the influence of a chiral auxiliary during a photoreaction. In this study this prediction has been realized with the guest pyridone systems **1a**–**e**, appended with the chiral auxiliary α-methylbenzyl amide (Scheme 1) in OA.[16–18] The position of the methyl group on the pyridyl ring was changed with the hope that it would influence the orientation of the guest, and thereby the free space, within the OA cavity. Prior studies with molecules like 4,4′-dimethylstilbene and dibenzyl ketone (Fig. 2) that are comparable in dimension to **1a**–**e** assured us accommodation of these guests inside OA cavity. Binding properties of compounds **1a**–**e** with OA were examined by NMR spectroscopy prior to initiating the photochemical studies. Both NMR and photochemical results are presented in this report.

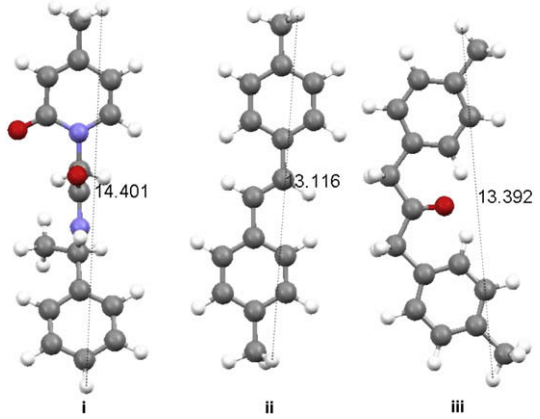

Figure 2. Ball and stick representation (i) of **1c**, (ii) 4,4′-dimethyl-*trans*-stilbene, and (iii) 4,4′-dimethyl dibenzyl ketone showing the relative dimensions of each molecule in an extended conformation.

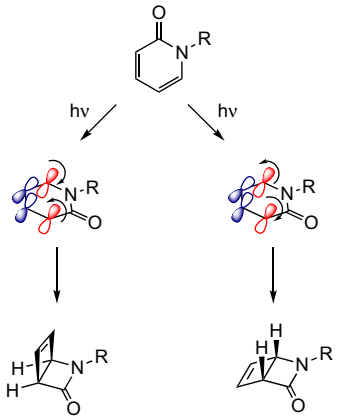

Scheme 2. Mechanism of the 4e disrotatory cyclization reaction of pyridone.

The probe molecules **1a–e** undergo concerted 4e disrotatory photocyclization in the excited singlet state. The mechanism of the photocyclization reaction is shown in Scheme 2. Planar achiral pyridone undergoes disrotatory cyclization (via two modes: in and out rotation) to yield the chiral 2-azabicyclo[2.2.0]hex-5-en-3-one. The products distinguished by the stereochemistry at the ring junction exist as enantiomers. Note that the planar reactant becomes bent (~110°) in the product. In a homogeneous environment, the cyclization occurs by both modes of rotation with equal efficiency. In a supramolecular chiral assembly, the host could provide torquoselectivity during the disrotatory cyclization process thus possibly leading to chiral enrichment on the photocyclized product.[19–21] Since the OA capsule is non-chiral, the photocyclization had to be influenced either through co-inclusion of a chiral inductor within the achiral capsule or through a chiral auxiliary co-valently linked to the reactant molecule. Our unsuccessful attempts at the former approach led us to explore the chiral auxiliary strategy that we had previously exploited in zeolites and crystals. This led us to investigate the photobehavior of pyridones **1a–e** within OA capsule. The results presented here highlight the influence of chiral auxiliary on the photocyclization when the reaction space is tightly controlled. Although the observed high de is remarkable we still do not fully understand the mechanics of the restricted space of the OA capsule in bringing about an interaction between the chiral auxiliary and the reaction center. We plan to continue to explore the origin and rules of chiral induction in photochemical reactions within the restricted space of OA capsule.

2. Results

2.1. Preparation and characterization of 1a–e@OA_2 complexes

Methyl-substituted pyridones **1b–e** were synthesized and their complexation behavior within OA was examined. The procedure for synthesis of these compounds is presented in the experimental section. Complexes of OA and pyridones **1a–e** were prepared using the following general procedure. A known volume of the guest from a stock solution in CD_3CN was transferred to a sample vial. The solvent was evaporated in a stream of air. To the solid pyridone thus deposited in the vial, solution of OA in buffered D_2O (2 equiv OA, 5×10^{-3} M solution) was added and the mixture stirred for 30 min.

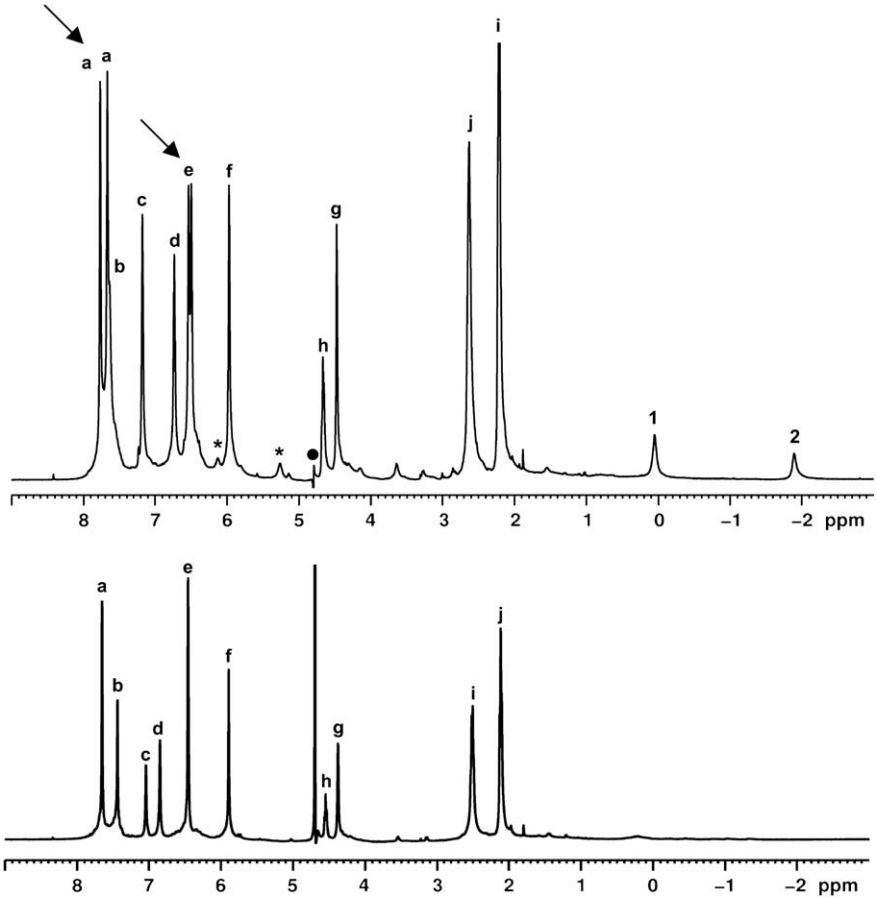

Figure 3. (bottom) ^{1}H NMR spectra (500 MHz, 298 K, buffered D_2O) of OA (10^{-3} M in 10^{-2} M $Na_2B_4O_7$) and **1b**@OA_2 in 1:0.5 ratio (5×10^{-3} M solution of OA in $Na_2B_4O_7/D_2O$) (top). The two methyl group signals of **1b** are marked as shown in Figure 8. Host hydrogens are labeled as shown in Figure 1.

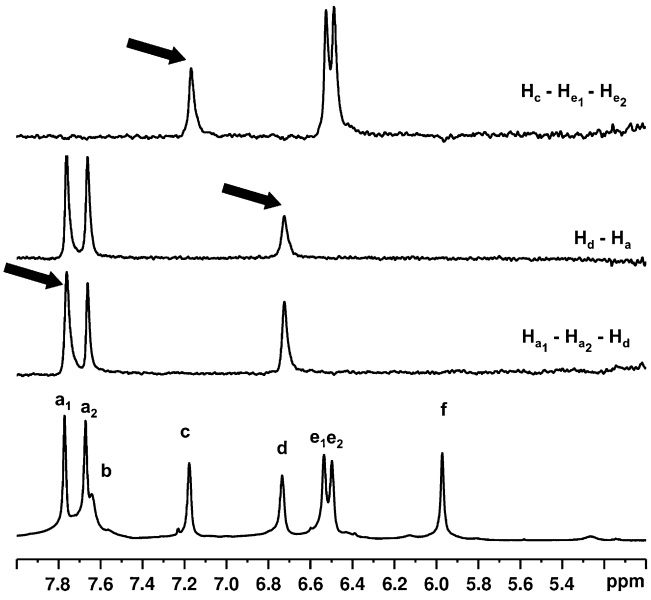

Figure 4. Partial 1D selective TOCSY NMR spectra (500 MHz, 298 K, D_2O, 0.12 s mixing time) of **1b**@OA_2 complex (5×10^{-3} M OA and 5×10^{-2} M $Na_2B_4O_7$) showing OA signals. Signal that is being irradiated is marked with an arrow. Observed TOCSY correlations (H_c–H_e, H_d–H_a, and H_a–H_d) are shown in the right.

Formation of host–guest complexes was monitored by ^{1}H NMR spectroscopy. To characterize the nature of complexes formed, Total Correlation Spectroscopy (TOCSY), Nuclear Overhauser Effect Spectroscopy (NOESY), and Diffusion Ordered Spectroscopy (DOSY) experiments were carried out.[22,23] In this section we present the NMR spectra relating to **1b**@OA_2 complex only. ^{1}H NMR spectra of other four complexes are provided in Supplementary data. ^{1}H NMR spectra of free OA and **1b**@OA_2 complex are shown in Figure 3 and 1D TOCSY and NOESY spectra are shown in Figures 4 and 5, respectively. NMR signals of aromatic and alkyl parts of OA complexes of **1a**–**e** are provided in Figures 6 and 7, respectively.

2.2. Stoichiometry of the complex

Host–guest ratio of the complex was established by two methods. Firstly, when greater than 0.5 equiv of the guest was

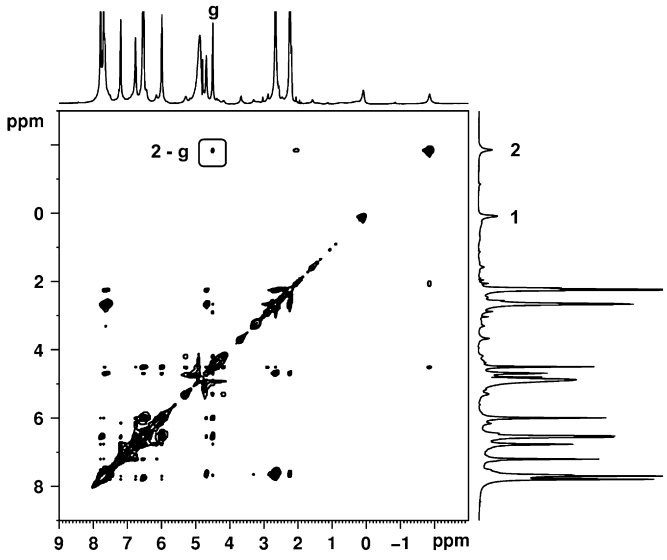

Figure 5. NOESY NMR spectrum (500 MHz, 298 K, D_2O, 0.5 s mixing time) of **1b**@OA_2 complex (5×10^{-3} M OA and 5×10^{-2} M $Na_2B_4O_7$).

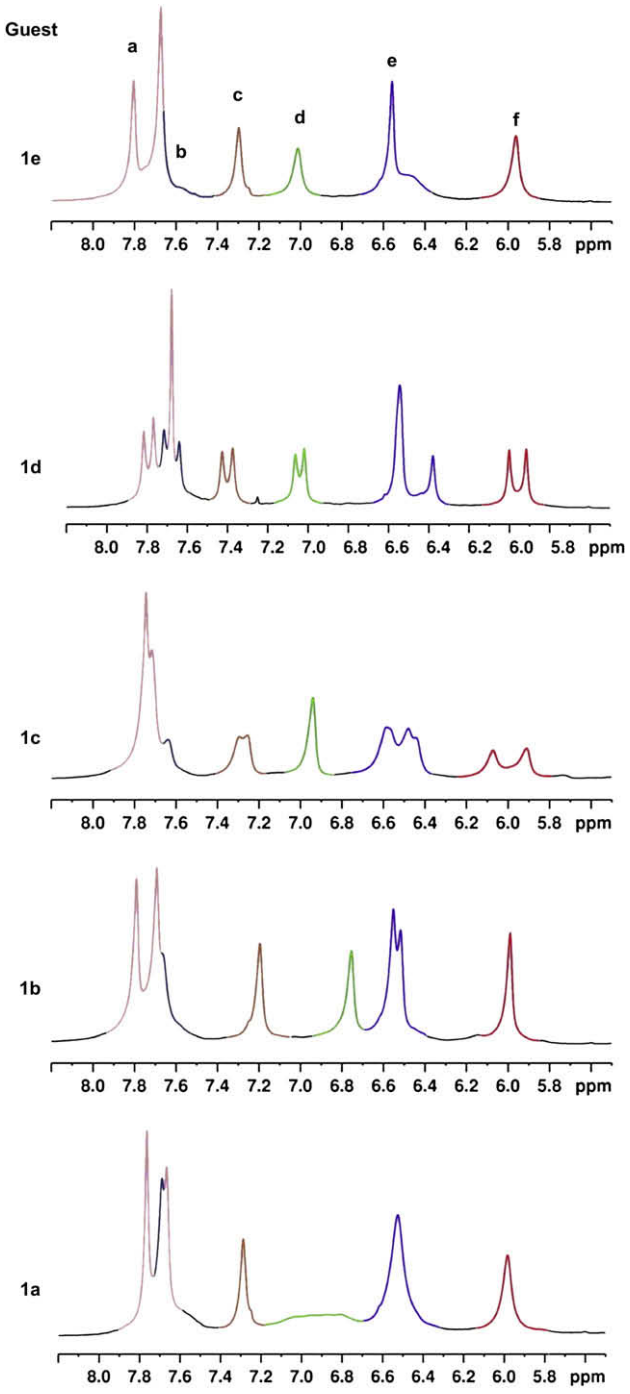

Figure 6. Partial ^{1}H NMR spectra (500 MHz, D_2O) showing the aromatic signals of the complex formed between OA and (i) **1a**, (ii) **1b**, (iii) **1c**, (iv) **1d**, and (v) **1e**. Each host signal is shown in different color as labeled in (v).

added to 1 equiv of OA solution, the solution became turbid indicating presence of free undissolved guest. No signals due to the uncomplexed guests were recorded in the ^{1}H NMR. Integration of the ^{1}H NMR spectrum of the complex at this stage showed a 2:1 host to guest ratio. Secondly, DOSY experiments were performed to identify the diffusion constants (D) of the complexes. The calculated diffusion coefficients in the units of 10^{-10} m^2 s^{-1} are 1.32 (**1a**@OA_2), 1.27 (**1b**@OA_2), 1.26 (**1c**@OA_2), 1.29 (**1d**@OA_2), and 1.35 (**1e**@OA_2). The measured diffusion coefficients were lower than that of free OA (1.88×10^{-10} m^2s^{-1}) and were comparable to the 2:1 host–guest complexes formed between OA and guests like dibenzyl

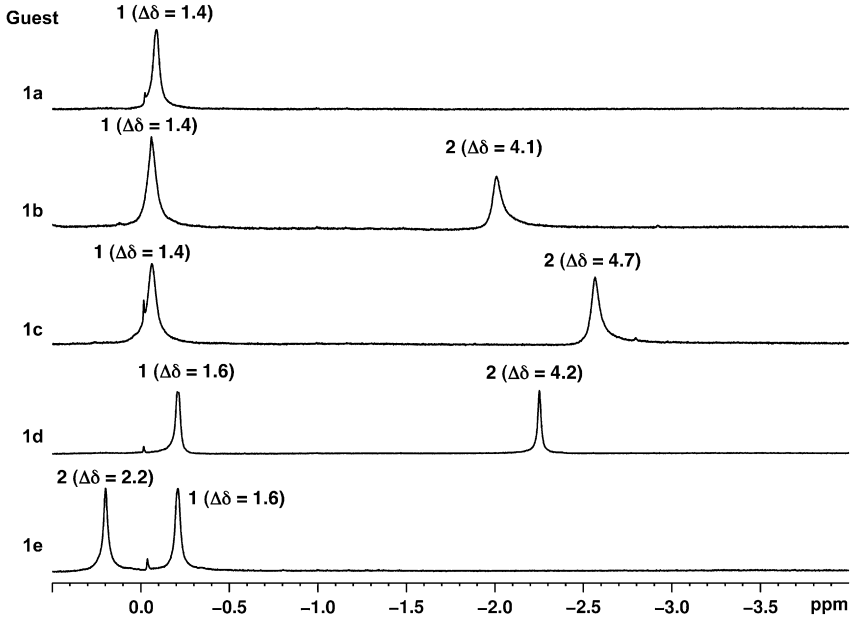

Figure 7. Selected regions of the ^{1}H NMR spectra (500 MHz, D_2O, 5×10^{-3} M OA, and 5×10^{-2} M sodium tetraborate) showing the aliphatic regions of OA complexes of **1a**, **1b**, **1c**, **1d**, and **1e**. Methyl groups of the chiral auxiliary and of the pyridone ring are labeled 1 and 2, respectively, as shown in Figure 8. Change in chemical shift upon binding to OA with respect to the NMR spectrum recorded in $CDCl_3$ ($\Delta\delta$) is also shown for each signal.

ketone. In the DOSY NMR spectra (Supplementary data), both the host and the guest signals show similar diffusion coefficients, confirming that the complexes formed were stable in the NMR time scale.

Further analysis of the NMR spectra of the complexes is divided into two sections, one concerning the guest and the other of the host. With the host–guest ratio of 2:1 we visualize the complex has a capsular structure and refer to the complex as a capsule in the text. The capsule is made up of two host cavities. Since addition of more than half an equivalent of the guest to 1 equiv of the host resulted in turbidity, binding constant measurements could not be carried out. Further, addition of more than half an equivalent of guest did not result in any new peaks indicating that no free guest remained in solution. Also, during the titration experiments no peak shifts were observed suggesting that at 5 mM all the complexes assembled and disassembled slowly (but close to, vide infra) on the NMR time scale.

2.3. Effect of host binding on the NMR spectra of the guest

As anticipated, magnetic shielding by the aromatic walls of the host induced upfield shifts of the guest signals. Analysis of the high field region was especially useful with this set of guests. Shown in Figure 7 are the partial ^{1}H NMR spectra (0 to −4 ppm) of the complexes formed by guests **1a**–**e**. Chemical shifts of the methyl signals from the chiral auxiliary are in the same region in all five spectra. This observation reveals that for all the different guests, the methyl groups present in the chiral auxiliary are in a similar position inside the capsule.

Chemical shifts of signals corresponding to the methyl group on the pyridone ring were affected to different extents. Difference in chemical shifts of the methyl signals in $CDCl_3$ and when bound to octa acid ($\Delta\delta$) is also shown in Figure 7. The maximum shift of 4.7 ppm was observed for **1c** (Fig. 7). Such a large shift of the methyl signal denotes strong shielding because it resides in the narrower region of the capsule where aromatic walls of the host converge. The shielding effect is lesser with the methyl groups of **1b** and **1d** (4.2 ppm each). Pyridyl methyl of **1e** was the least shielded (2.2 ppm) denoting its position in the central wider region of the capsule.

2.4. Effect of guest binding on the NMR spectra of the host

In the NMR spectrum of free OA (Fig. 3, bottom), six aromatic signals (signals a–f) can be seen. Theoretically, in the ternary complex formed between a guest (**1a**–**e**) and two OA, two kinds of signal splitting are expected. First, the complex is chiral and so protons that are enantiomeric in the free host (H_a and H_e) become diastereotopic in the complex. Second, because each molecule of OA accommodates different parts of the guest, the two OA 'hemispheres' (top and bottom, Fig. 1) are non-equivalent. Hence, there should be two signals for protons H_b, H_c, H_d, and H_f (the top/bottom divide), whilst protons H_a and H_e should be split into four signals (diastereotopicity and the top/bottom divide). The complex with **1b**@OA_2 does not show this degree of splitting; only two signals are split into two. To help identify these signals, a 1D selective TOCSY NMR of the complex with **1b** was collected. Figure 4 shows the partial spectrum. In OA, three sets of interacting aromatic hydrogens H_a and H_d, H_c and H_e, and H_b and H_f (Fig. 1) are present. TOCSY correlations were observed for two of these: H_a and H_d, and H_c and H_e. Thus, in the complex with **1b**@OA_2 only the signals from H_a and H_e are seen to split (Fig. 3, top, Fig. 4) and there is no observable top/bottom divide for H_b, H_c, H_d, and H_f. It is not possible to identify with this experiment whether the splitting of H_a and H_e is due to their inherent diastereotopicity, or because the top/bottom divide leads to relatively large splitting for these particular protons and the assembly and disassembly rate of the capsule is such that only the splitting of these protons is observable (k_c=2.22$\Delta\nu$). 1D TOCSY spectra of the complexes between OA with other guests (Supplementary data) were used to identify aromatic signals of each host and are collected in Figure 6.

The position of the methyl substituent on the pyridone ring in **1a**–**e** had a significant impact on the NMR spectra of the host. Among the five complexes, host signals were split most with guests **1c** and **1d** (Fig. 6). While the diastereotopic H_a signals appeared as doublets in every complex, multiplicity of other aromatic hydrogen

signals was not consistent. Figure 6 shows the aromatic region of the NMR spectra of each complex. A brief description of each complex is provided below.

(i) In **1a**@OA_2 complex, two signals were observed for H_a. The signal from H_d was also broadened significantly. Other host signals were not split.
(ii) Relatively sharp, host signals were observed for **1b**@OA_2 complex. However, only diastereotopic H_a and H_e signals were split into doublets.
(iii) The complexes **1c**@OA_2 showed a good deal of splitting, but overall the peaks were poorly resolved.
(iv) The complexes **1d**@OA_2 showed the theoretical splitting for all the signals, but overlap of the H_a and H_b signals, and overlap among the four signals for H_e, was evident.
(v) With the **1e**@OA_2 complex, only H_a signal was split. Unlike the complexes formed with **1c** and **1d**, one set of signals for H_c, H_d, and H_f was observed.

These results demonstrate that from the perspective of the aromatic signals of the host, assembly and disassembly are close to the NMR time scale. It is only because of the large shifts experienced by the methyl groups of the guest that assembly and disassembly appear slow on the NMR time scale (k_c=2.22$\Delta\nu$) from their perspective.

Although only the methyl signals of the guest were observable (other guest signals were either obscured by those from the host or too small to readily identify) some useful NOE interactions between host and guest were observed. These provided insight into the relative position of the guest inside the capsule. While the NOESY spectrum of **1a**@OA_2 lacked any informative correlations, in the NOESY NMR spectrum of the other guests (Fig. 5 and Supplementary data) NOEs between the inward pointing H_g signal of the host and the pyridyl methyl of the guest were evident. In contrast, the benzyl methyl of **1c**, **1d**, and **1e** shows NOE correlations with 'equatorially' positioned H_d of the host. This result is significant in assigning the two methyl signals of **1e**@OA_2 complex. In the **1e**@OA_2 complex, NOE interaction between H_g and only one guest methyl is observed, and it is assigned as the pyridyl methyl. The NOESY interactions in complexes of guests **1b**–**e** are pictorially represented in Figures 8 and 9. In the two figures two possible conformations of each pyridone ring are presented. However, of the two, the intramolecular hydrogen-bonded conformations shown in Figure 9 are expected to be favored within the non-polar OA capsule. All further discussions use this conformation to represent **1** within OA capsule.

Based on NMR analysis, we visualize the structures of the complex formed between OA and guests **1a**–**e** as in Figure 10. In summary, NMR experiments demonstrated that OA formed stable 2:1 complexes with the guests **1a**–**e**, in which the guest adopts a general orientation shown in Figure 10. It should be apparent that we represent all five molecules in intramolecular hydrogen-bonded conformations within the OA capsule. The only difference between these host–guest structures is the location of the methyl group in each case within the OA capsule.

2.5. Dynamic behavior of the guests inside the capsule

In the proposed structures of the complexes (Fig. 10), each OA molecule of the capsule accommodates either the phenyl ring or the pyridone ring of the guest. To investigate the dynamics of guest movement, variable temperature NMR spectra were recorded. Figure 11 shows the NMR spectra of **1d**@OA_2 complex recorded between 278 K and 313 K. Below room temperature, signals were observed to sharpen, while at higher temperatures, most signals moved toward coalescence. This is in agreement with the observation that from the perspective of the host aromatic protons assembly and disassembly are close to the NMR time scale. Unfortunately, due to experimental limitations spectra could not be recorded at temperatures higher than 313 K.

In addition to the above assembly–disassembly, rotation of a bound guest molecule is possible along the longitudinal (polar) axis and along the equatorial axis of the complex (Fig. 12). ^{1}H NMR data reported here suggest dynamic behavior along both axes. For ease of visualization, the two OA molecules are distinguished using two colors (red and blue) in Figure 12. Guest rotation along the long axis (axis II in Fig. 12) is generally rapid. The four subunits of OA are not distinguished in the NMR spectra due to the rotation of the guest along the long axis.

Rotation of the guest along the equatorial axis of the host (axis 1 in Fig. 12) is relatively challenged by the available space inside the capsule, especially with guests like **1a**–**e**. However, with guests like 4-methylanisole,[24] acetophenone,[25] and quioniline[25] incarcerated in smaller hemicarceplexes, rotation of the guest along the short axis of the host has been reported. Such a guest rotation remained a possibility in our guest–host complexes also.

In the NOESY NMR spectrum of **1d**@OA_2 complex (Fig. 13), NOESY correlations between the methyl group 2 of **1d** and both the H_g signals of the host supported the exchange of guest between the two OA molecules that form the capsule. In the absence of rotation along axis-2, each ring of the guest must be confined to the cavity of one host molecule, and hence, NOE correlation for the methyl group must also be restricted to only one H_g signal. Rotation of the guest is rapid enough that signals of equal intensity are observed in the NOESY NMR spectrum. However, NOE relationship with both H_g signals could also be due to the occurrence of assembly–disassembly in the NMR time scale. Given that we have collected data at long mixing time scale (0.5 s) this can't be ruled out. We plan to carry out NOE experiments at several mixing time to ascertain what is responsible for the NOE correlation with H_g protons of the top and bottom parts of the capsule. Absence of clearly split H_g signals in the NMR spectrum of other complexes limits our analysis to this example.

In summary, formation of stable 2:1 complexes of OA and guests **1a**–**e** was established by NMR spectroscopy. The differential magnetic shielding effect of the host on the guest resonances was illustrated with the chemical shifts of the two methyl group signals of the guests. Dynamic behavior of the bound guest was also identified using NOESY and TOCSY NMR analysis of the complexes. Note that the NMR data provide information on the rotational motion in a much longer time scale than excited state time scale ($\sim 10^{-9}$ s). In the excited state time scale, most likely, the guest molecule is stationary and the photobehavior could be understood on the basis of the average structures presented in Figure 10.

2.6. Results of photochemical studies

^{1}H NMR spectra of the complexes of guests **1a**–**e** and OA suggested a possibility of co-existence of 2:1 and 1:1 host–guest complexes at 298 K, when less than 10^{-3} M solution of OA was used. To increase the binding and the stability of the complex, the photocyclization reactions were carried out using 5×10^{-3} M OA solutions (2.5×10^{-3} M guest). As indicated in the earlier section at this concentration only 2:1 complex was present in solution. Products of irradiations were analyzed by HPLC using chiral stationary phase column. In the photolysis studies, compounds A and B represent the photoproducts formed from the disrotatory/conrotatory cyclization of the pyridone. When analyzed by HPLC, the first product signal was arbitrarily assigned as A and the second signal as B. The structures of A and B are as shown in Scheme 2. No attempt was made to ascertain the absolute configuration of the

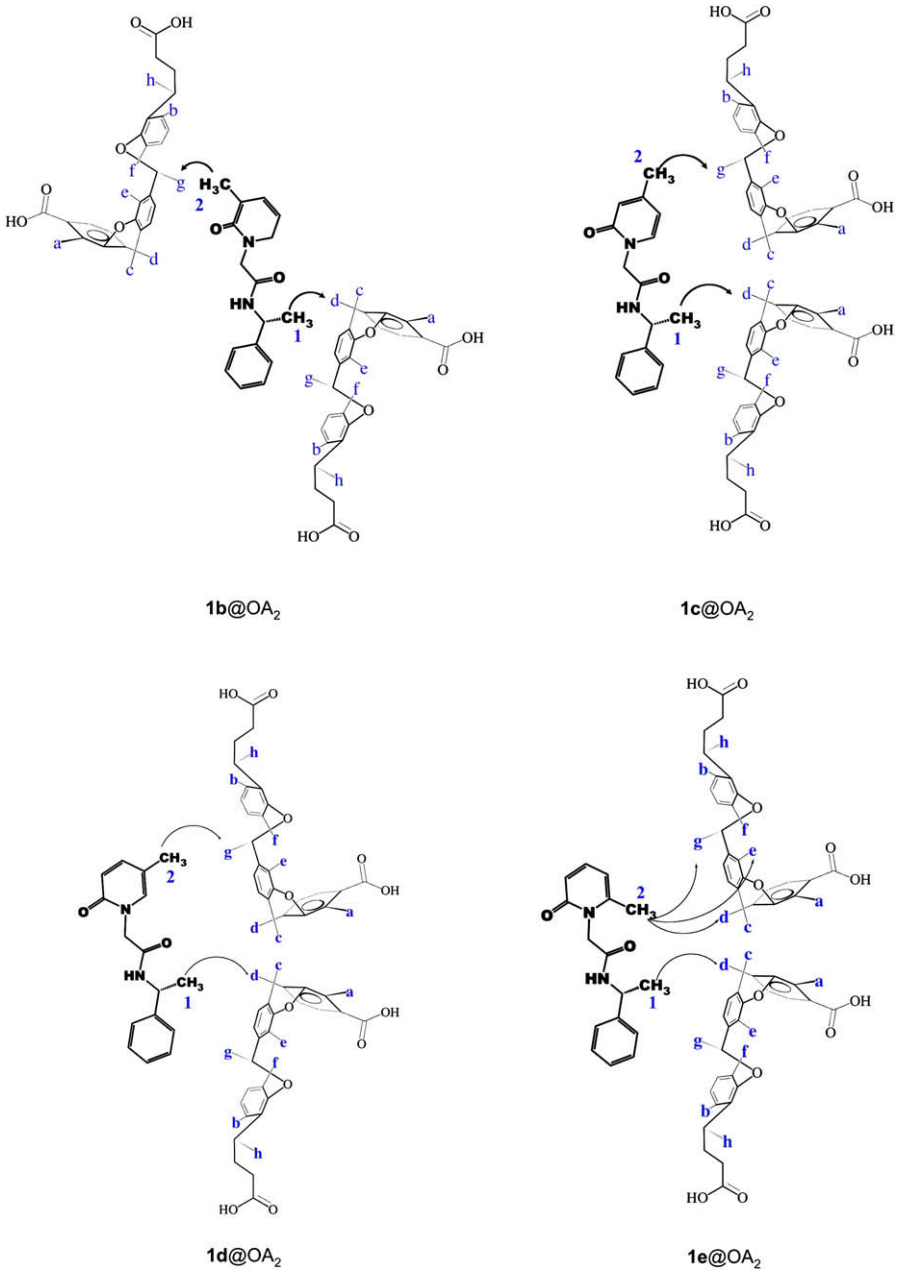

Figure 8. Pictorial representation of NOE correlations observed between OA and guest molecules. Also see Figure 9.

photoproducts. However, since the products were not distinguished from one another, we did not assign the structures specifically in Scheme 2. Similarly, HPLC analysis showed that product A (i.e., the first product signal) was formed in excess in all substrates.

Our initial studies with **1a** appended with either (*S*) or (*R*) α-methylbenzyl amine chiral auxiliary were encouraging. These gave 16% and 17% excess of one diastereomer as monitored by HPLC. Although the de obtained was small, difference between acetonitrile solution without OA (1% de) and water with OA (17% de) suggested that OA is capable of forcing an interaction between the chiral auxiliary and reaction center. Prompted by this result we investigated the photochemistry of methylated systems **1b**–**e**. Choice of methylation was dictated by our previous observation with methylstilbenes and methylcyclohexene bound to OA, which suggested that the guest's methyl substituent could help better anchor the guest in the OA cavity.

The first methyl-substituted pyridone analyzed as OA complex was **1c**, where the methyl substituent is *para* to the nitrogen and hence, *para* to the chiral auxiliary. The observed diastereoselectivity increased from 17% observed for **1a** to 41% for **1c**. Further enhancement of de was achieved by changing the reaction temperature to 278 K. The selectivity increased to 64% from 41% at 298 K. Encouraged by the observations, other methyl-substituted derivatives were examined. Results of photochemical investigation with guests **1a**–**e** in acetonitrile and as OA complex are summarized in Table 1. All guests were solids and not soluble in water or borate buffer. Hence irradiation of these guests (in the absence of OA) was not performed in buffer solutions and comparison was made to the results in acetonitrile.

Introduction of methyl substituent had considerable impact on the photochemistry of the bound guest. As with **1c**, not only did the photochemistry of the guests show a remarkable diastereoselectivity after methyl substitution, the observed selectivity also

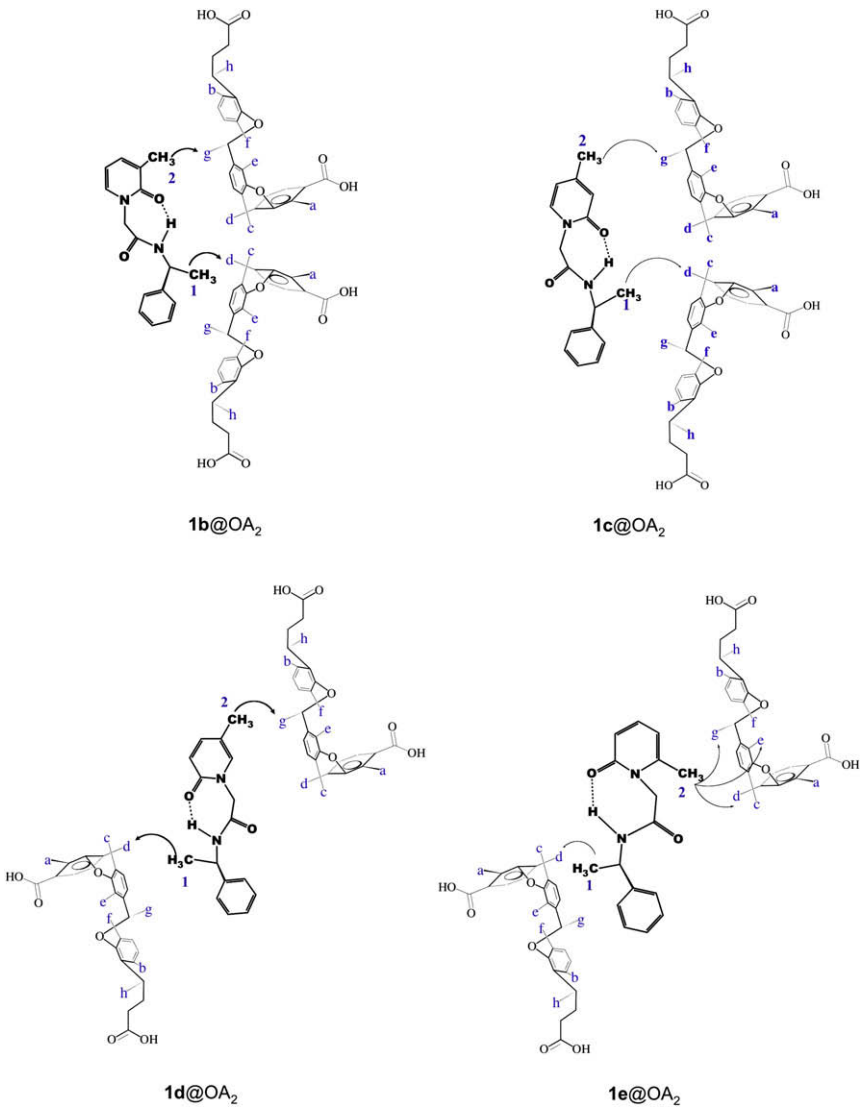

Figure 9. Pictorial representation of NOE correlations observed between OA and each guest. The guests are represented by intramolecular hydrogen-bonded structures.

varied with the position of the substituent. In general, the diastereoselectivity was greater when the reaction was carried out at 278 K (5 °C). While the highest selectivity was observed with 3-methyl derivative (**1b**), the 73% preference for one diastereomer at 298 K increased to 92% at 278 K in the case of **1b**@OA_2. The diastereoselectivity obtained from room temperature irradiation of **1d**@OA_2 was 60% and it improved to 70% at 278 K. Finally, with methyl substituent at the *ortho*-position (**1e**) 50% and 56% selectivity were observed at 298 K and 278 K, respectively.

We believe that the observed diastereoselectivity is not controlled entirely by anyone participant (chiral auxiliary, the host, and/or the methyl substituent), but by a combination of all three. Control experiments carried out in the absence of anyone of the three 'participants' confirmed this hypothesis. When the reaction is

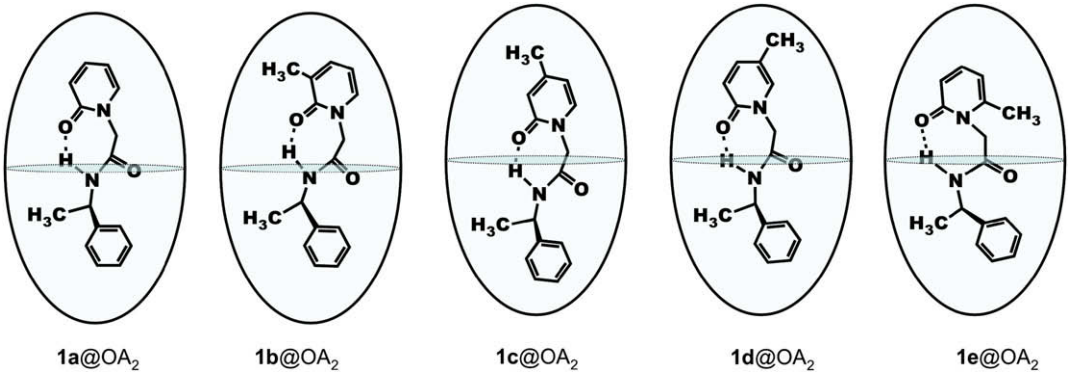

Figure 10. Proposed structures of 2:1 complexes formed between OA and guests **1a**–**e**.

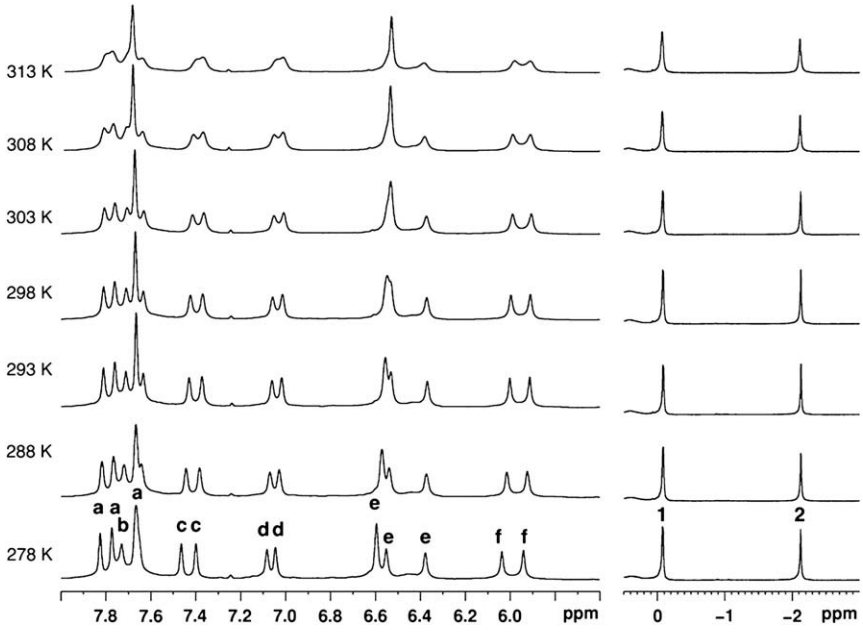

Figure 11. Partial ^{1}H NMR spectra (500 MHz, D_2O) of **1d**@OA_2 complex (5×10^{-3} M OA and 5×10^{-2} M $Na_2B_4O_7$) recorded at temperatures between 278 K and 313 K. The temperature at which each spectrum was recorded is shown on the left side of the spectrum. Host signals are labeled a–f as shown in Figure 1. Guest methyl signals are labeled 1 and 2 as shown in Figure 8. Intensity (*Y*-axis) of the methyl signals is greater than the intensity of the aromatic region.

performed in acetonitrile (i.e., in the absence of the host, but in the presence of the auxiliary and the methyl group), the product was racemic. Similarly, selectivity was low from **1a** bound to OA, illustrating the importance of the methyl substituent. To ensure that the reaction is not affected by OA alone (in the absence of the chiral auxiliary), photolysis of OA complexes of *N*-propyl-2-pyridone and *N*-pentyl-2-pyridone was carried out. A racemic mixture of photoproducts was isolated. Based on these control experiments, we conclude that the three groups viz., OA, chiral auxiliary, and the methyl substituent have a synergetic effect on the photocyclization process.

3. Discussion

The results of photochemical reactions pose the following questions: (a) Why there is a difference in de between isotropic solution and OA capsule? (b) How does the position of the methyl on the pyridone ring control the extent of de? (c) How does the chiral communication occur between the chiral auxiliary and the reaction center within the OA capsule?

We have previously established that high chiral induction on a variety of photoreactions could be achieved within a zeolite, a medium where cation$\cdots\pi$ interaction restricts the conformational flexibility of the chiral auxiliary.[26–30] We believe that similar restriction of the chiral auxiliary occurs within the OA capsule. However, within the OA capsule no weak interaction is expected as in zeolite and therefore the conformational restriction must result from tight inclusion. Thus the free space within the capsule is an important parameter to be considered during the chiral induction process within the OA capsule. To gain an understanding of this parameter we need to have knowledge of the guest structure within the OA capsule.

The NMR data have provided an insight into the structure of the guest (in the NMR time scale) within the OA capsule. Although we have inferred from the NMR data that the guest within OA capsule

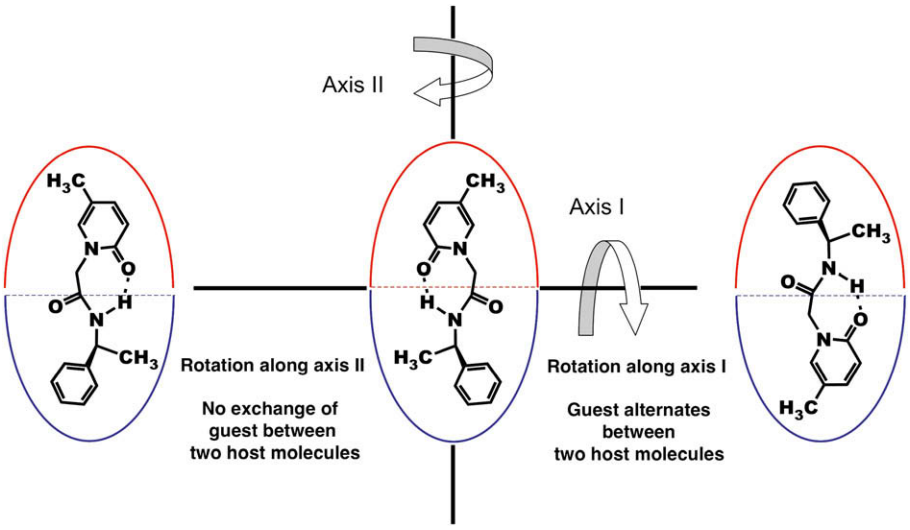

Figure 12. Representation of the two possible rotations of a guest bound to the host capsule.

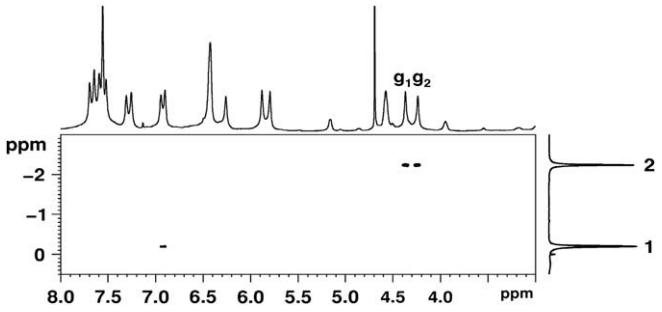

Figure 13. Partial NOESY NMR spectrum (500 MHz, 298 K, buffered D_2O, 0.5 s mixing time) of **1d**@OA_2 complex (5×10^{-3} M OA and 5×10^{-2} M $Na_2B_4O_7$) showing the interactions between the two methyl groups of the guest and the host.

is mobile in the NMR time scale the guest is expected to be rigid and not to undergo rotational motions within the capsule in the excited state (S_1, $<10^{-9}$ s) time scale. We believe that the host–guest structure shown in Figure 10 is a good starting point for understanding the chiral induction within the OA capsule.

The ^{1}H NMR chemical shift of the methyl-1 (on the chiral auxiliary) is nearly identical (δ approx. –0.15 ppm, Fig. 7) in all five guests suggesting that its position remains almost the same within OA capsule in all five structures, most likely in the broader region slightly below the middle portion of the capsule. Thus the chiral auxiliary part (α-methylbenzyl amide) is envisioned to be at one half of the capsule with the α-methyl in the mid-region and the benzyl stretching to the bottom. The ^{1}H NMR chemical shifts of the methyl-2 (on the pyridone ring) vary between 0.2 and −2.5 ppm (Fig. 7). The maximal and minimal shifts for **1c** and **1e**, respectively, suggest that in the former it is at the deepest part and in the latter it is in the mid-region of the capsule. Nearly identical shifts in **1d** and **1b** suggest that the methyl-2 in these two cases is slightly below the mid-region of the cavity. Based on the ^{1}H NMR chemical shift of the methyl-2 we believe that the pyridone ring resides in one half of the capsule such that pyridone N–R (R=chiral auxiliary) bond is parallel to the long axis of the capsule. Similarly, based on the near identical chemical shift of methyl-1 in pyridones **1b**–**e** we believe that the benzyl part of the chiral auxiliary is anchored into the other half of the capsule and the Ph–C(CH_3)H bond is parallel to the long axis of the capsule. The mid-part of the molecule (CH_2–CO–NH–CHR′) connecting the pyridone and the chiral auxiliary (α-methyl benzyl group) probably adopting a folded structure remain in the mid-region of the capsule.

Table 1
Diastereomeric excess[a,b] observed in the cyclization reaction of guests **1a**–**e** in acetonitrile and as OA complexes at different temperatures

Guest	Medium	% de[b] at two temperatures	
		298 K	278 K
1a	CH_3CN	1 (A)	—
	OA complex	17 (A)	21 (A)
1b	CH_3CN	4 (A)	—
	OA complex	73 (A)	92 (A)
1c	CH_3CN	2 (B)	—
	OA complex	41(A)	64 (A)
1d	CH_3CN	0	—
	OA complex	60 (A)	70 (A)
1e	CH_3CN	2 (A)	—
	OA complex	50 (A)	56 (A)
1f	CH_3CN	2	
	OA complex	2	

[a] The results are based on HPLC analysis using chiral column and are average of at least three independent runs.
[b] The first photoproduct signal is assigned A and the second signal is assigned as B. % de is calculated using the ratio [area of A−area of B]×100/[area of A+area of B].

In Figure 14 rotations that are more likely and less likely within the capsule are also indicated. Rotations (rotations 1, 2, and 3 in Fig. 14) that involve large positional change of the phenyl or pyridone rings that are anchored at the two hemispheres of the capsule are unlikely. As long as the CH_2–CO–NH–CHR′ adopts a folded structure in the mid-region of the capsule, rotation-4 is likely to flip the molecule between the hydrogen-bonded and non-hydrogen-bonded structures (Figs. 8 and 9). Considering that the intramolecular hydrogen-bonded structure is more stable such a rotation is unlikely within the capsule. Thus while in solution phase rotations of various single bonds would be expected to freely occur, within the OA capsule many such rotations would be restricted. Thus while in an isotropic solution the chiral auxiliary is expected to have conformational freedom and the chiral center is unlikely to be rigid with respect to the reaction site, within OA capsule the opposite holds. Thus, the role of OA is not only to retain the substrate (pyridone ring) and the chiral auxiliary in close proximity in its cavity for an extended period of time, but also to hold the chiral group in a single conformation with respect to the reaction site. We believe that this important difference is likely to be the origin of chiral induction within the OA capsule.

Compared to unsubstituted pyridone system **1a**, methylated pyridone systems **1b**–**e** gave higher chiral induction in the photoproducts (21% vs 56–92%). Clearly the methyl group, independent of its location in the pyridyl ring, has a significant impact on the chiral induction (Table 1). We speculate that this most likely results from the snug fit of the methyl substitued pyridone (with respect to the unmethylated **1a**) within the capsule. The presence of greater free space within the **1a**@OA_2 capsule does not seem to significantly differentiate the inward and outward motions during the disrotatory cyclization of the pyridone ring (Scheme 2). Results with pyridone **1f** (Table 1) provided further support to the above rationale. The chiral auxiliary part in **1f** is much smaller than that in **1b**–**e**. Therefore this molecule would be expected to fit loosely leaving considerable free space within the OA capsule. As expected based on free space model this molecule would be expected to yield low de. In fact **1f** yields 0% de both in acetonitrile solution and in OA capsule at room temperature.

Our answer to ‘Why the de depends on the position of the methyl group on the pyridone ring’ admittedly, is speculative. As stated above the pyridone part occupies one half of the capsule such that N–R (R=chiral auxiliary) bond is parallel to the long axis of the capsule. With the dimensions of the differently methyl-substituted pyridones provided in Figure 15 it is easy to visualize how the width of the pyridone part would determine how deep it would penetrate the capsule. For example, the narrower **1c** would go deeper than **1e**, which is wider at the top. Such a positioning would leave considerable unoccupied space below the pyridone ring in **1e**. Pyridone **1e** gives the lowest de (56%) amongst the four methylated pyridones. This possibly suggests that larger free space in the capsule allows for ring closure by either mode shown in Scheme 2 leading to moderate de. The second lowest de (64%) with **1c** expected to fit snugly within the capsule makes us wonder if a tight fit, like too loose one, is not conducive to distinguish the two modes of rotations. The best de is obtained with **1b** and **1d** (92% and 70%) that have similar width (Fig. 15). These two molecules as indicated in Figures 8 and 9 would be expected to have their pyridone rings midway between the widest and narrowest regions of the capsule with a free space intermediary between those of **1c** and **1e**. This delicate balance between free space and tight fit may be responsible for the observed higher de in these two cases, especially in **1b**. Overall we believe that free space plays a critical role in the chiral induction process within the capsule. At this stage we are unable to estimate the exact amount of free space and link it mechanistically to the extent of de.

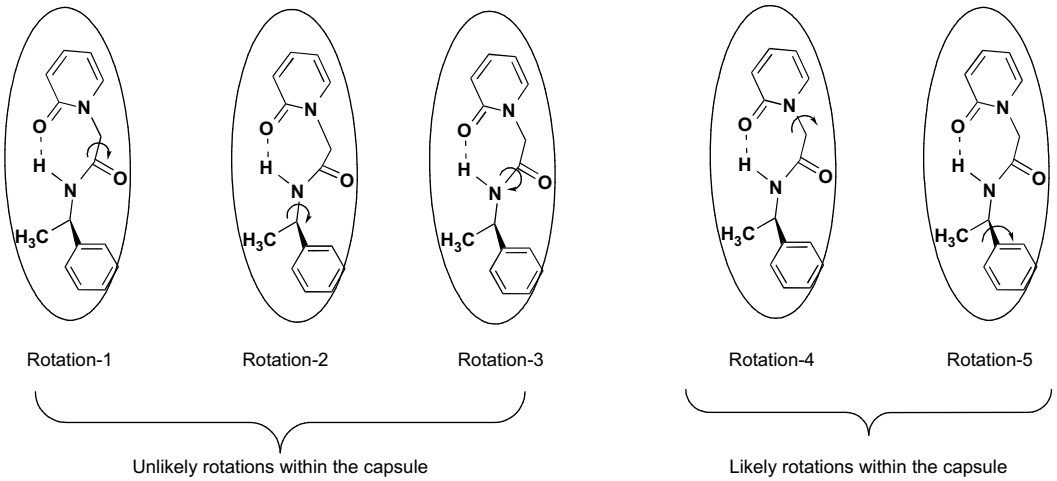

Figure 14. Probable and improbable rotational motions of **1a** within OA capsule. This model is applicable to other systems as well.

4. Summary

We have achieved significant chiral induction (92%) during the photocyclization of pyridones within a hydrophobic capsule. Such high chiral induction in a hydrophobic capsule, to our knowledge, is unprecedented. Controlling free space and freedom of rotation are major factors in deciding the efficiency of chirality transfer between the chiral auxiliary and the reaction site. For instance, reactions in solid state yield better selectivity than in solution state due to the denser packing of molecules curbing the substrate's motion in the former. Similarly, one can expect the substrate bound to OA to experience greater influence of the host when the packing is efficient. At this stage 'How the chiral communication occurs between the chiral auxiliary and the reaction center within the OA capsule' remains a question. Given that this is our inaugural publication on chiral induction within a hydrophobic capsule we are optimistic that with time we will be able to better understand this phenomenon. We are optimistic that with time this initial result of ours on chiral induction within a hydrophobic capsule would provide a better understanding of this phenomenon.

5. Experimental

5.1. General methods

Host octa acid was synthesized and characterized using literature procedures. Synthesis of compounds **1a**–**e** using reported procedures is explained below. ^{1}H NMR spectra were recorded using Bruker Avance 300, 400 or 500 MHz spectrometers at 298 K unless mentioned otherwise. Photoproducts of **1a**–**e** were separated by HPLC analysis using Rainin HPLC instrument fitted with Chiralcel AD column and hexane and 2-propanol as eluants.

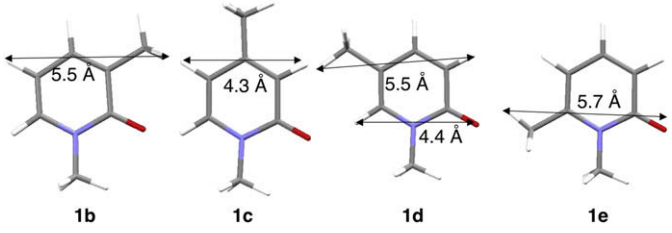

Figure 15. Width of the pyridone rings of the four methyl-substituted guests.

5.2. General procedure for synthesis of 1a–e

5.2.1. (R)-2-Bromo-N-(1-phenylethyl)ethanamide

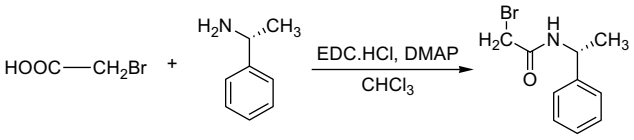

To a solution of bromoacetic acid (2.52 mmol, 1.1 equiv) in $CHCl_3$, *N*-ethyl-*N*′-(3-dimethylaminopropyl)carbodiimide hydrochloride (2.5 mmol, 1.1 equiv), and 4-(dimethylamino)pyridine (0.5 mmol) were added. The solution was stirred for 30 min at ambient temperature. (*R*)-α-Methylbenzyl amine (2.3 mmol, 1 equiv) was added in one portion and the reaction mixture was stirred at room temperature for further 16 h. The reaction was quenched by adding 10 mL of water. The organic layer was separated and washed with three portions of water, dried over anhydrous sodium sulfate, and concentrated. Excess bromoacetic acid and the coupling reagents were removed by flash chromatography (silica gel, chloroform, methanol) to isolate the product as white solid.

5.2.2. (R)-2-(3-Methyl-2-oxopyridin-1(2H)-yl)-N-(1-phenylethyl)ethanamide ***1b***

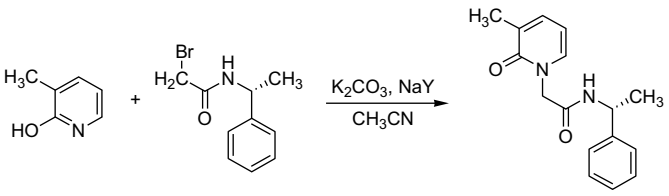

Reagents used for this coupling required activation prior to synthesis. NaY zeolite was dried in an oven for at least 5 h at 500 °C. Potassium carbonate was dried at 150 °C for 3 h. 3-Methyl-2-hydroxypyridone (1 equiv) in acetonitrile was refluxed with activated zeolite and potassium carbonate (2 equiv) for 1 h, following which ((*R*)-2-bromo-*N*-(1-phenylethyl)ethanamide) was added. After overnight stirring at reflux, the solution was filtered while warm to remove the inorganic solids. Acetonitrile was distilled and the crude mass was purified by passing through a silica column with chloroform and methanol as eluants. The product was characterized by ^{1}H NMR and ^{13}C NMR spectroscopy. Similar procedure

was used for synthesis of compounds **1a** and **1c–e** using the appropriate 2-hydroxypyridone.

5.2.3. NMR characterization

Compound **1a**: ^{1}H NMR (500 MHz, $CDCl_3$) δ 7.69 (s, 1H), 7.39 (s, 2H), 7.26 (m, 4H), 6.59 (d, J=8.5 Hz, 1H), 6.25 (d, J=8.5 Hz, 1H), 5.03 (t, J=6 Hz, 1H), 4.68 (d, J=14 Hz, 1H), 4.48 (d, J=14 Hz, 1H), 1.43 (d, J=5.5 Hz, 3H). ^{13}C NMR (100 MHz, $CDCl_3$) δ 166.5, 163.2, 143.5, 140.9, 139, 128.9, 127.5, 126.4, 120.8, 107.2, 53.7, 49.5, 22.5.

Compound **1b**: ^{1}H NMR (500 MHz, $CDCl_3$) δ 7.45 (s, 1H), 7.3 (m, 6H), 6.2 (t, 1H), 5.1 (t, 1H) 4.6 (s, 2H), 2.2 (s, 3H), 1.4 (d, 3H). ^{13}C NMR (100 MHz, $CDCl_3$) δ 166.8, 143.4, 138.1, 135.8, 130.3, 128.9, 127.5, 126.2, 107, 54.8, 49.5, 22.6, 17.5.

Compound **1c**: ^{1}H NMR (500 MHz, $CDCl_3$) δ 7.84 (s, 1H), 7.27–7.21 (m, 5H), 6.36 (s, 1H), 6.10 (d, J=6.5 Hz, 1H), 5.023 (t, J=7 Hz, 1H), 4.66 (d, J=14.5 Hz, 1H), 4.45 (d, J=14.5 Hz, 1H), 2.2 (s, 3H), 1.42 (d, J=6.5 Hz, 3H). ^{13}C NMR (100 MHz, $CDCl_3$) δ 166.8, 152.8, 143.5, 137.7, 128.9, 127.5, 126.4, 119.2, 109.7, 53.4, 49.5, 22.5, 21.7.

Compound **1d**: ^{1}H NMR (500 MHz, $CDCl_3$) δ 7.8 (d, 1H), 7.25 (m, 6H), 6.53 (t, J=9 Hz, 1H), 5.03 (q, J=7 Hz, 1H), 4.62 (t, J=14.5 Hz, 1H), 4.45 (q, J=9 Hz, 1H), 2.0 (s, 3H), 1.43 (d, J=6.5 Hz, 3H). ^{13}C NMR (100 MHz, $CDCl_3$) δ 166.8, 162.5, 143.6, 143.5, 136.3, 136.2, 128.9, 127.5, 126.3, 120.4, 116.3, 54.1, 49.5, 22.6, 17.3.

Compound **1e**: ^{1}H NMR (500 MHz, $CDCl_3$) δ 7.59 (s, 1H), 7.24 (m, 6H), 6.49 (d, J=8.5 Hz, 1H), 6.1 (d, J=6.5 Hz, 1H), 5.03 (t, J=7 Hz, 1H), 4.7 (s, 2H), 2.4 (s, 3H), 1.43 (d, J=7 Hz, 3H). ^{13}C NMR (100 MHz, $CDCl_3$) δ 167, 164.4, 147.3, 143.6, 140.2, 128.9, 127.5, 126.2, 117.6, 108, 49.2, 49.1, 22.6, 21.2.

5.3. Preparation and photolysis of complexes and isolation of the products

Irradiation of the substrates was carried out in CH_3CN solutions. Complex of **1a–1e** and octa acid was prepared using 5 mM solutions of octa acid containing 50 mM sodium tetraborate in D_2O. A stock solution of the guest dissolved in CD_3CN, typically in 1 mg/mL concentration was prepared. An aliquot of the stock solution corresponding to 0.5 equiv of octa acid was taken in a vial and the solvent was evaporated in a stream of air. Octa acid (0.6 mL, 5 mM solution) was added and the solution was stirred for 30 min. Complete solubilization of the guest was achieved at this time based on NMR analysis of the solution. The vial was sealed with a septum and nitrogen was bubbled through the solution for 30 min prior to irradiation. Irradiation was carried out to obtain 20–30% conversion (3–4 h). The photoproducts were extracted using $CHCl_3$ and analyzed by HPLC analysis and were compared with the photoproducts obtained when compounds **1a–e** were irradiated in CH_3CN.

5.4. Parameters for ^{1}H NMR, 1D selective TOCSY NMR, 2D NOESY NMR, and DOSY NMR analysis

Water suppressed ^{1}H NMR experiments were performed using presaturation technique with Bruker's pulse program *zgcppr*. 1D selective TOCSY NMR experiments were performed with Bruker's pulse sequence *selnogp.3*. The mixing time used for TOCSY experiments was 0.120 s. 2D NOESY experiments were performed with 0.5 s mixing time. DOSY NMR experiments were recorded using *stebpgp1s* sequence. ^{1}H NMR spectra of OA complexes of **1a**, **1c**, **1d**, and **1e** (27 figures in total) are provided in Supplementary data.

Acknowledgements

V.R. greatly appreciates the continuous encouragement, penetrating discussions, and critical comments by Professor R. S. H. Liu to whom this paper is dedicated. V.R. thanks the National Science Foundation, USA for financial support (CHE-0213042 and CHE-0531802). C.L.D.G. and B.C.G. thank the National Institute of Health (RO1 GM074031) for financial support.

Supplementary data

General experimental procedures and extensive NMR data of host–guest complexes are provided as electronic supplementary file (28 pages). Supplementary data associated with this article can be found in the online version, at doi:10.1016/j.tet.2009.01.110.

References and notes

1. Inoue, Y.; Ramamurthy, V. *Chiral Photochemistry*; Marcel Dekker: New York, NY, 2004.
2. Rau, H. In *Chiral Photochemistry*; Inoue, Y., Ramamurthy, V., Eds.; Marcell Dekker: New York, NY, 2004; Vol. 11, p 1.
3. Grosch, B.; Bach, T. In *Chiral Photochemistry*; Inoue, Y., Ramamurthy, V., Eds.; Marcel Dekker: New York, NY, 2004; pp 315–340.
4. Wada, T.; Inoue, Y. In *Chiral Photochemistry*; Inoue, Y., Ramamurthy, V., Eds.; Marcel Dekker: New York, NY, 2004; Vol. 11, pp 341–384.
5. Hoffmann, N.; Pete, J. P. In *Chiral Photochemistry*; Inoue, Y., Ramamurthy, V., Eds.; Marcel Dekker: New York, NY, 2004; Vol. 11, pp 179–233.
6. Inoue, Y. In *Chiral Photochemistry*; Inoue, Y., Ramamurthy, V., Eds.; Marcel Dekker: New York, NY, 2004; Vol. 11, pp 129–177.
7. Toda, F.; Tanaka, K.; Miyamoto, H. In *Understanding and Manipulating Excited-State Processes*; Ramamurthy, V., Schanze, K. S., Eds.; Marcel Dekker: New York, NY, 2001; Vol. 8, pp 385–425.
8. Sakamoto, M. In *Chiral Photochemistry*; Inoue, Y., Ramamurthy, V., Eds.; Marcel Dekker: New York, NY, 2004; Vol. 11, pp 415–461.
9. Scheffer, J. R. In *Chiral Photochemistry*; Inoue, Y., Ramamurthy, V., Eds.; Marcel Dekker: New York, NY, 2004; Vol. 11, pp 463–483.
10. Ramamurthy, V.; Natarajan, A.; Kaanumalle, L. S.; Karthikeyan, S.; Sivaguru, J.; Shailaja, J.; Joy, A. In *Chiral Photochemistry*; Ramamurthy, V., Inoue, Y., Eds.; Marcel Dekker: New York, NY, 2004; Vol. 11, pp 563–631.
11. Shailaja, J.; Karthikeyan, S.; Ramamurthy, V. *Tetrahedron Lett.* **2002**, *43*, 9335–9339.
12. Koodanjeri, S.; Ramamurthy, V. *Tetrahedron Lett.* **2002**, *43*, 9229–9232.
13. Koodanjeri, S.; Joy, A.; Ramamurthy, V. *Tetrahedron* **2000**, *56*, 7003–7009.
14. Gibb, C. L. D.; Gibb, B. C. *J. Am. Chem. Soc.* **2004**, *126*, 11408–11409.
15. Gibb, B. C. In *Organic Nanostructures*; Atwood, J. L., Steed, J. W., Eds.; VCH Verlag GmbH: Weinheim, 2008; pp 291–304.
16. Corey, E. J.; Streith, J. *J. Am. Chem. Soc.* **1964**, *86*, 950–951.
17. Toda, F.; Tanaka, K. *Tetrahedron Lett.* **1988**, *29*, 4299–4302.
18. Wu, L. C.; Cheer, C. J.; Olovsson, G.; Scheffer, J. R.; Trotter, J.; Wang, S. L.; Liao, F. L. *Tetrahedron Lett.* **1997**, *38*, 3135–3138.
19. Walker, M. J.; Hietbrink, B. N.; Thomas, I. B. E.; Nakamura, K.; Kallel, E. A.; Houk, K. N. *J. Org. Chem.* **2001**, *66*, 6669–6672.
20. Nakamura, K.; Houk, K. N. *J. Org. Chem.* **1995**, *60*, 686–691.
21. Dolbier, W. R.; Koroniak, H.; Houk, K. N.; Sheu, C. *Acc. Chem. Res.* **1996**, *29*, 471–477.
22. Natarajan, A.; Kaanumalle, L. S.; Jockusch, S.; Gibb, C. L. D.; Gibb, B. C.; Turro, N. J.; Ramamurthy, V. *J. Am. Chem. Soc.* **2007**, *129*, 4132–4133.
23. Gibb, C. L. D.; Sundaresan, A. K.; Ramamurthy, V.; Gibb, B. C. *J. Am. Chem. Soc.* **2008**, *130*, 4069–4080.
24. Helgeson, R. C.; Knobler, C. B.; Cram, D. J. *J. Am. Chem. Soc.* **1997**, *119*, 3229–3244.
25. Place, D.; Brown, J.; Deshayes, K. *Tetrahedron Lett.* **1998**, *39*, 5915–5918.
26. Sivaguru, J.; Natarajan, A.; Kaanumalle, L. S.; Shailaja, J.; Uppili, S.; Joy, A.; Ramamurthy, V. *Acc. Chem. Res.* **2003**, *36*, 509–521.
27. Sivasubramanian, K.; Kaanumalle, L. S.; Uppili, S.; Ramamurthy, V. *Org. Biomol. Chem.* **2007**, *5*, 1569–1576.
28. Natarajan, A.; Ramamurthy, V. *Org. Biomol. Chem.* **2006**, *4*, 4533–4542.
29. Joy, A.; Kaanumalle, L. S.; Ramamurthy, V. *Org. Biomol. Chem.* **2005**, *3*, 3045–3053.
30. Sivaguru, J.; Sunoj, R. B.; Wada, T.; Origane, Y.; Inoue, Y.; Ramamurthy, V. *J. Org. Chem.* **2004**, *69*, 6533–6547.